MOLECULAR DOCKING AND QUANTUM CHEMICAL CALCULATION OF 4-[(2, 4- DICHLORO PHENYL) AMINO] 2- METHYLIDENE 4-OXOBUTANOIC ACID BY DENSITY FUNCTIONAL THEORY

Abstract

4-[(2, 4- dichloro phenyl) amino] 2-methylidene 4-oxobutanoic acid (DPAB) is a promising antiviral agent. An unified computational strategy merging molecular mechanics and quantum mechanics methods was utilised in the current investigation for explaining the intricate relationship between DPAB and its inhibitors at the atomic level. FT-IR and FT-Raman spectroscopy have been utilised to look into the spectroscopic characteristics of 4-[(2, 4- dichloro phenyl) amino] 2-methylidene 4-oxobutanoic acid molecule. In the solid phase, FT-IR (4000-400 cm-1) and FT-Raman (3500-10 cm-1) spectra were noticed. DFT (B3LYP) using 6311++G(d, p) and 6311+G(d, p) basis set computations yielded the molecule's structural and spectroscopic data. The molecule's structure was properly optimised, based on the potential energy distribution (PED) of the vibrational modes, spectra were calculated, and fundamental vibrations were given.

Keywords: FT-IR, FT-Raman, DFT studies, Docking.

Authors

G. Mahalakshmi
Associate Professor
Department of Physics
Government Arts College (A)
Karur, Tamilnadu, India.

K. Vanasundari
Associate Professor
Department of Physics
Arignar Anna Government Arts College
Musiri, Tamilnadu, India.

V. Balachandran
Associate Professor
Department of Physics
Arignar Anna Government Arts College
Musiri, Tamilnadu,India.

I. INTRODUCTION

We live in a decade of rapid antiviral drug development. Various kinds of antiviral pharmaceuticals have been legally authorised for use in the prevention and management of certain viral diseases [1-4]. An antiviral agent that treats a disease or puts a virus down by blocking viral invasion or procreation. In recent decades, the relevance of novel broad-spectrum antiviral drugs has been highlighted as way of offering greater defence against a range of viruses while limiting resistance risks and lowering the costs that accompany creating remedies unique to a specific virus. “Antiviral substances with high efficacy, low resistance, and low harm remain mysterious, and this remains an important area of medicinal development. Due to its distinctive three-dimensional geometrical characteristics, DPAB has been recognized as one of the ideal chemo types of antiviral drugs development. Density functional theory has been employed this time around to carry out molecular docking and quantum chemistry simulations on 4-[(2, 4- dichlrophenyl) amino] 2- methylidene 4-oxo butanoicacid. Natural bond orbital inquiry assessed the redistribution of electron density in various bonding and antibonding orbitals, together with stabilisation energies, to offer unambiguous evidence of stabilisation resulting from hyper-conjugation of a variety of intra-atomic bonds. Nonlinear properties, Mulliken atomic charges, and Fukui functions have been explored. Molecular docking is a sophisticated computer process to identify a ligand's affinity for proteins which has proved exceedingly helpful and efficient in modern structure-based drug design. The structure of the target protein can be acquired via the protein data bank (PDB) protocol. The ligand protein molecular docking tackle can foresee the ligand's preferred placement with with regard to the protein to enable to make a stable complex and its multiple forms”.

.

II. COMPUTATIONAL DETAILS

The title compound was estimated making use of the Gaussian 09 programme [5] along with Becke's three parameter hybrid model via the Lee-Yang-Parr correlation functional (B3LYP) strategy. The 6-311++G(d, p) and 6- 311+G(d, p) basis sets were implemented to figure out the chemical structure and vibrational wavenumbers. To view most effective structures, the Gauss View software was employed [6]. Molecular electrostatic potentials along with natural population analyses have been computed at the precise same level. The descending density gradient of noncovalent interactions can be plotted using Multiwfn [7]. The Autodock-vina software has been employed to carry out molecular docking studies [8].

III. RESULTS AND DISCUSSIONS

Geometrical Structures: The molecular structure of DPAB, as well as the atom numbering, can be determined using the Gaussian 09 software and are depicted in Fig.1. The global minimum energy derived by DFT structural optimisation using the 6-311+G(d, p) premise for the DPAB was -1632.5 a.u. The physical characteristics of the molecule i-e bond lengths and bond angles are illustrated in Table 1. There is no discernible distinction between the 6-311++G(d, p) basis sets of the strategies. The C-H bond lengths of CH2 groups and the Phenyl ring are determined to be 1.09 and 1.08, respectively, which are in more harmony with the literature [9].

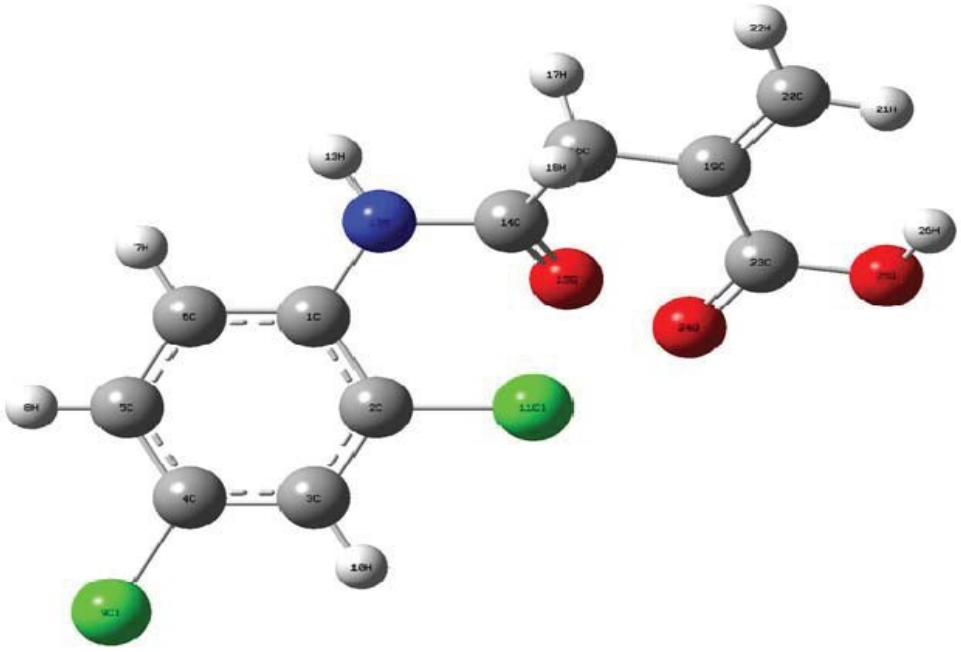

Figure 1: Optimized geometrical structure of [(2,4-dichlorophenyl)amino]2-methylidene4-oxobutanoicacid

The C-C bond lengths in the present article are computed from 1.39 to 1.41, exhibiting greater compatibility with experimental data and literature [10]. As demonstrated that certain discrepancies amongst anticipated and empirical results could possibly be attributed to the fact that calculations originated from gas phase while reality data are gathered in solid phase. The bond angles between Cl11-O24-C23 (149.43), C1-N12-C14 (127.91), N12-C14-O15 (125.22), and C19-C20-H21 (123.03) display detachment in this molecule. In addition, it highlights the more prominent electronegative characteristic of oxygen and nitrogen atoms. The optimised Carbon-Nitrogen bond length is 1.37, thus being in accordance with the literature [11]. The ring Carbon-Carbon-Carbonbond angles obtained from the range of 117.46°121.97° show an adequate agreement with experimental findings [12]. When C-Cl bonds replace those in a C-H package, the bond length grows significantly. The Cl atom substitution induces the bond lengths of C2-Cl11 (1.76), C4-Cl9 (1.76) to be longer than the rest of the bonds in the ring.

1. **Vibrational Spectral Analysis:** The intention of this section of the research is to assign vibrations so that they may be compared to equivalent chemicals and theoretical simulations. The title molecule comprises of 26 atoms with 72 normal modes of vibration and C1 point group symmetry. “Table 2 summarises the whole assessment regarding basic modes of vibration with authentic and theoretical frequencies, as well as the PED of the title molecule using the DFT/B3LYP tackle using split-valence basis sets (6-311++G(d, p) and (6-311+G(d, p). Figures 2 and 3 demonstrate the actual and probable infrared and Raman spectra, respectively. The calculated spectra are presented for comparison. The vibrational spectral analysis of the title chemical may be characterized using extreme frequencies. Aromatic compounds typically exhibit several weak bands in the region 3100-3000 cm-1 due to aromatic C-H stretching vibrations [13]. As a consequence, the current work identifies the C-H stretching vibrations of DPAB at 3098,

3085, 3021[6-311++G(d, p)] and 3095, 3071, 3015 cm-1 [6-311+G(d, p)]. Experimental vibrations have been found at 3188, 3074 (FT-IR), and 3072 cm-1 (FT-Raman). In the 13001000 cm-1 and 1000-750 cm-1 areas, the bands that result from C-H in-plane and out-of-plane bending vibration interacting with C-C stretching vibration show up as a pattern of medium weak intensity sharp bands [14]. C-H in-plane bending vibrations are detected in DPAB at 1348, 1317, 1183 (FT-IR), and 1148 cm-1, respectively.

Hypothetical bending vibrations have been designated as CH out-plane bending vibrations at 977, 874, 855, and 841cm-1 [(6-311++G(d, p)]. Carbon-carbon stretching vibrations have been allocated at 1579, 1519, cm-1 (FT-IR) and 1603, 1293 cm-1 (FT-Raman) in this sample. The vibrational modes of scissoring, rocking, wagging, and twisting are depicted by the methylene group (CH2) of the heading molecule, which functions as a link with the COOH group to the phenyl ring. The ranges of the symmetric and asymmetric C-H stretching vibrations of CH2 are 2865 and 2936 cm-1, correspondingly [7]. The reported FT-Raman band at 2993cm-1 belongs to the CH2 asymmetric stretching mode, with derived wavenumbers of 3089, 2995 cm-1 (6-311G+(d, P) and 3088, 2991 (6-311G++(d, P). The CH2 scissoring vibrations arise as a medium intensity band in the 1490, 1435 cm-1 geographic area [15]. The Methyl bending is found to be considerably mixed with the methyl bending modes of the phenyl ring, and the predominant methyl bending is assigned at 1476, 1455 cm-1 (6-311++G(d, p) with experimental FT-IR band at 1474 and 1454 cm-1". The CH2 wagging mode has been placed at 1287 (88%) and 1233 cm-1 (94%), which equates well with the observed bands in the FT-IR spectra at 1286 and 1231 cm-1. The predominant mode of motion for the CH2 rocking vibrational gestures is assigned at 867 and 788 cm-1, which coincides with well with experimental data (866 cm-1 in FT-IR and FT-Raman). In the wavelength region of 1150-850 cm-1, absorption bands triggered by C-N symmetric stretching modes have been witnessed [16,17].

The reported spectra of 6-311++G(d, p) and 6-311+G(d, p) at 1208 and 1206 cm-1, correspondingly, have been attributed the C-N stretching pattern of DAPB. The high group frequency of the C=O structural unit has been acknowledged as a stretching vibration. Almost every carbonyl compounds have an extremely powerful and condensed peak between 1800 and 1600 cm-[18].Because the many tied groups are very polar, they yield an immense infrared absorption band in the 1700 cm-11800 cm-1 region. Carbon-oxygen double bonds occur via the - bonding of carbon and oxygen. a combination of various electro negativities of the carbon and oxygen atoms, the bonding electrons are not distributed roughly among the atoms [19]. The C=O stretching vibration appears as a strong band in FT-Raman at 1682 cm-1, and the derived wavenumbers are 1718 and 1683 cm-1, with PED contributions of 82% and 70%, respectively. The empirically obtained FT-IR and FT-Raman bands agree well with our theoretical values. Jian et al. [20] observed the C=O stretching vibrations of 1-acetyl-3-(2, 4-dichloro-5-fluro-phenyl)-5-phenylpyrazoline at 1660 cm-1 (exp) and 1708 cm-1 (6-31G*).

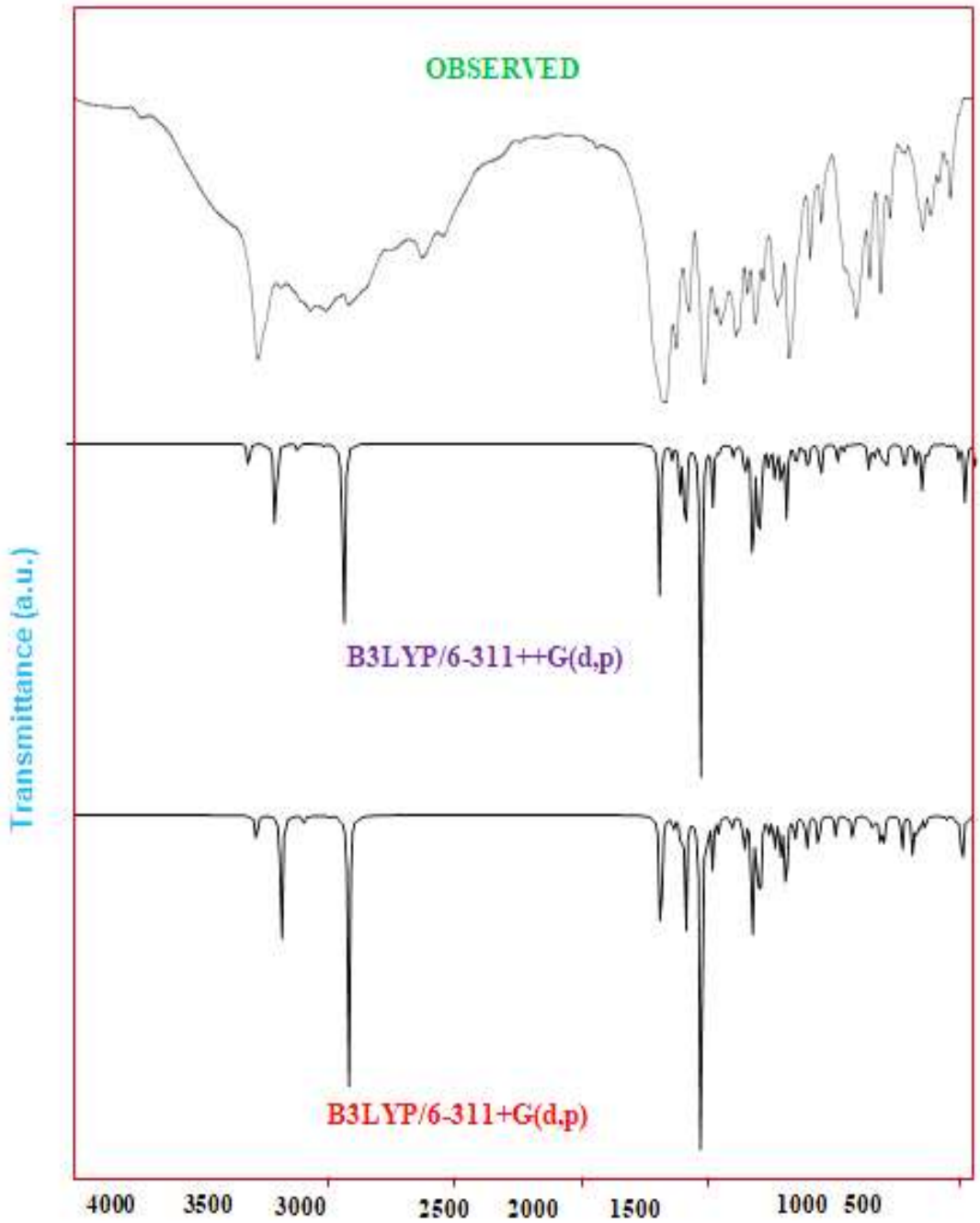

Figure 2: FT-IR spectrum of [(2,4-dichlrophenyl) amino] 2-methylidene 4-oxobutanoicacid]

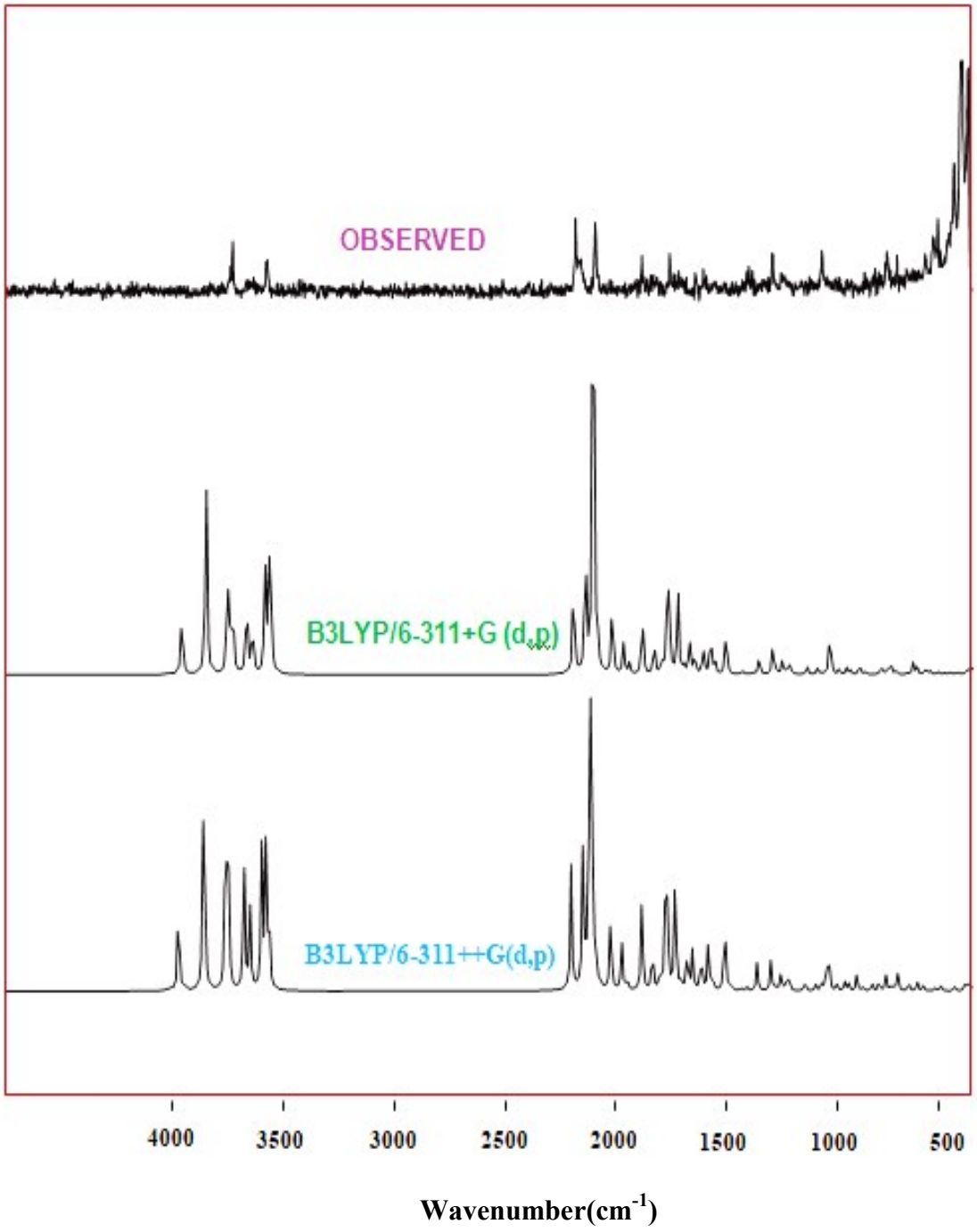

Figure 3: FT-Raman spectrum of -[(2,4-dichlrophenyl) amino] 2-methylidene4-oxobutanoic acid]

"Since the loss of structural symmetry and the presence of a heavy element on the molecule's perimeter make vibrational mixing conceivable, it is important to take into account the vibrational mode of the connection between the ring and the halogen atom in this situation [21].

The region between 750 and 580 cm-1 is where C-Cl absorption is seen [22]. DPAB C-Cl stretching mode is therefore responsible for the band seen in the IR spectra at 656 cm-1 and FT-Raman at 669 cm-1.At 547 cm-1 (FT-IR), the C-Cl in-plane bending mode was seen, and it may also be detected at 515, 465 cm-1 [6-311++G(d, p)] and 511, 422 cm-1 [6-311+G(d, p)].The predicted values for C-Cl out-of-plane bending are 190,138 (6- 311G+(d, p)), and 192,141 cm-1 (6- 311G++(d, p)).

2. **NBO:** The NBO 3.1 programme [23], as implemented in the Gaussian 09 package, was used to perform natural bond orbital analysis (NBO) at the B3LYP/6-311++G(d, p) level basis set. NBO analysis is implemented to figure out every potential relationship between full (donor) Lewis type NBOs and empty (acceptor) non- Lewis type NBOs, as well as to judge perturbation theory. Some of the necessary donor-acceptor interactions along with associated second-order perturbation energies E(2) can be clarified by the second-order NBO study of stabilisation energy E(2). Tables 3 and 4 indicate the most crucial donor-acceptor interactions. The intention of NBO analysis is to convey the impact of inter and between molecules bonding. It also illustrates how to distinguish between charge transfer or hyper-conjugative interactions in a chemical system. B.Through resonances, the O24 atom's lone pair of electrons associated with anti-bonding orbitals *C2 -Cl11, *C14-O15, *C19-C23, *C23-O24, and *C23-O25, leading with significant conjugative stabilisation energies of 6.35, 28.71, 6.08, 9.74, and 19.57 Kcal/mol. In addition, in DPAB, the lone pair LPO25 associated with the anti-bonding orbitals of C23-O24, C14-O15, C19-C20, and C14-O15 through hyper-conjugation to the pi-anti-bonding orbital. The stabilising energies for this type of hyper-conjugation are 28.45, 8.17, 132.45, and 26.09 Kcal/mol. The energy variance among interacting atoms pertains to the stabilisation of orbital relationships. As a result, among which the most significant stabilising interactions occur between dominant donors and acceptors [24]. The subsequently formed complex had been stabilised by 18.82, 9.11, 28.71, and 28.45 kcal/mol of LPO15*N12-C14, LPO24*C2-Cl11, and LPO25C23-O24, respectively.

3. **Mulliken Atomic Charges:** The charge distribution on a molecule has an enormous impact on its vibrational spectrum. Chemistry rides on the atomic charge of molecules. For instance, charge transfer and electro negativity equalisation in chemical reactions have both been outlined with the theory of atomic charge [25-26]. The 6-311++G(d, p) basis set and the DFT/B3LYP approach are utilised to identify the Mulliken atomic charges. The predicted reactive atomic charges serve a vital part in the utilisation of molecular quantum mechanical predictions. The heading compound's Mulliken atomic charges are illustrated and provided in Table 5. Research results imply that the electron density varies whenever chlorine atoms are incorporated into the phenyl ring. The distribution of charges for CH2 groups is the same. The positive charge on hydrogen atoms renders them acceptors. As donor atoms, oxygen (O25= 0.54 a.u.) and nitrogen (N12= 0.64 a.u.) have a strong negative charge.

4. **MEP:** Picture 8.5 exhibits an interactive 3D model of the molecular electrostatic potential map surface for DPAB. The use of visualisation helps you grasp the reaction across the molecule's structure and active site. It has been employed for recognising electrophilic and nucleophilic reactivity sites, as well as hydrogen bonding interactions. The MEP [27] has been demonstrated for DPAB because it provide information on the whole electron structure of the molecule and depicts zones of nucleophilicity and electrophilicity on the

molecular surface. Positive electrostatic potential (represented by blue) corresponds to the repulsion of a proton by atomic nuclei in the region of low electron density, whilst negative electrostatic potential (expressed by red) corresponds to the attraction of protein by centred electron density in the molecule. The two massive negative potential zones adjacent to the nitrogen atom of the phenyl ring and the oxygen atom of the carbonyl group show obvious in the MEP of DPAB. The greatest positive and negative potential values displayed on the MEP map in the molecular plane are +9.623 a.u and -9.623 a.u, respectively, and these values correspond to the electrophilic and nucleophilic domains.

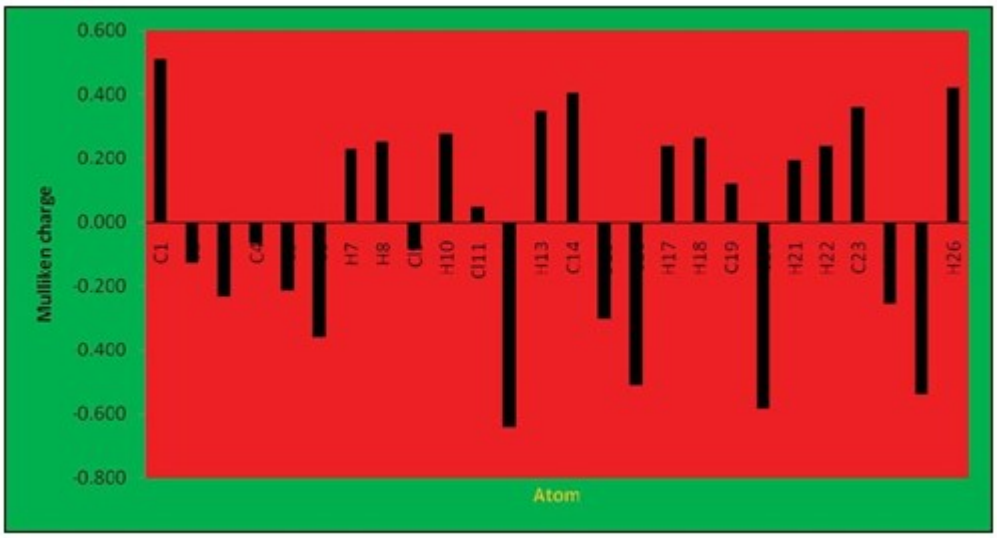

(a)

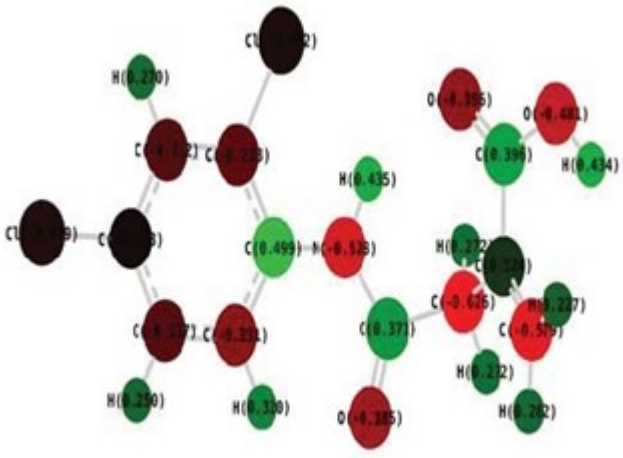

(b)

Figure 4: (a)The histogram of calculated Mulliken charge and(b)Atoms with their mulliken charge values of [(2,4-dichlrophenyl)amino] 2-methylidene 4-oxobutanoicacid]

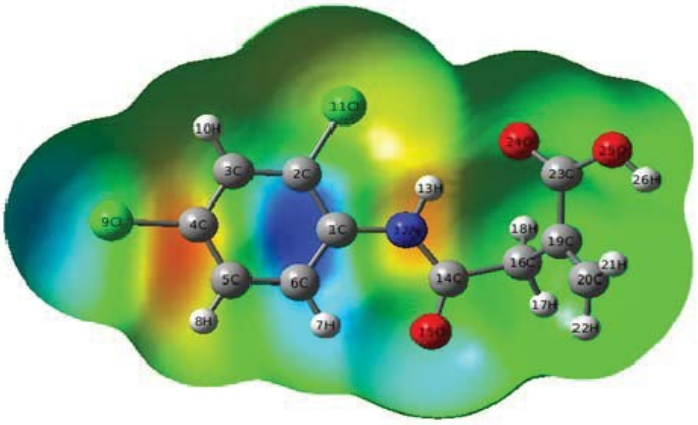

Figure 5: The 3D surface map of [(2,4-dichlorophenyl)amino] 2-methylidene4-oxobutanoicacid

5. **Frontier Molecular Orbitals and their Related Molecular Properties:** The outermost molecule (HOMOLUMO) orbital plays a role in the overall picture of electric and optical features, UV-Vis spectra, and chemical interactions [27]. The highest unoccupied molecular orbital (HOMO) and the lowest unoccupied molecular orbital (LUMO) play essential functions in quantum chemistry. The HOMO orbital mostly serves as an electron donor whereas the LUMO orbital mainly functions as an electron acceptor. Based on molecular orbital coefficient analyses utilising the DFT/B3LYP/6-311G++ (d, p) optimised structure, the electronic transitions from the HOMO-2, HOMO-1, and HOMO to the LUMO arise predominantly from n-* transitions due to the frontier molecular orbitals comprise mainly of the p atomic orbitals. For the molecular form of DPAB in the gas phase, the distributions and energies of the HOMO-2, HOMO-1, HOMO, LUMO and LUMO-2, LUMO+2 orbitals are provided in Fig 6. Though the negative phase is green, the positive phase is red. With the exception of the CH2 groups, the LUMO in the title chemical has been decentralised within the whole system. The HOMO-LUMO transition consequently entails an evolution of electron density from the phenyl rings to the methyl groups. Quantum chemical attributes are anticipated from the HOMO and LUMO orbital energies. Using the HOMO and LUMO orbital energies, ionisation energy and electron affinity may be stated as I=EHOMO and A=ELUMO, respectfully. The difference between LUMO and HOMO energy is directly linked to the hardness. The harder the molecule, the wider the HOMO-LUMO energy gap. For the forecast of global hardness, the relation = (ELUMOEHOMO)/2 will be used. A chemical system's stability and hardness have been are linked. The reciprocal of the chemical system's hardness decides how soft it is. The reciprocal of the hardness, or 1/, reflects what the softness is. The global electrophilicity index is provided by the electronic chemical potential, which has a value equal to (ELUMO+EHOMO)/2 when the electron affinity and ionisation energy are combined. This index assesses the stability of energy once the system gained a supplementary electronic charge from the atmosphere around it. The aforementioned parameters are listed in Table.8.6 for the substance referred to in the title. The high excitation states (2.41eV), excellent stability, and substantial chemical hardness for the title of the compound can be unambiguously demonstrated by the energy disparity between the HOMO-LUMO gap.

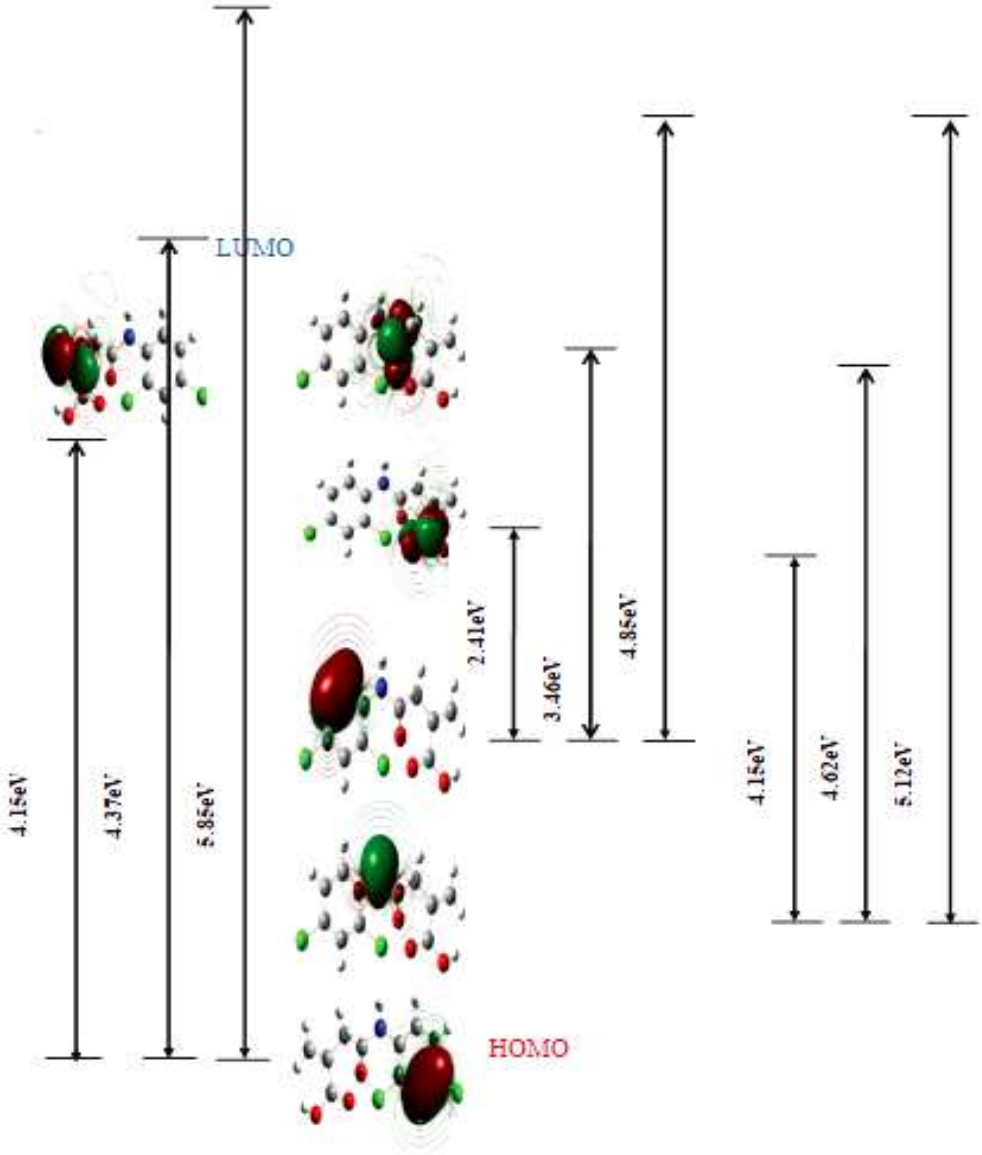

Figure 6: HOMO-LUMO plot of [(2,4-dichlorophenyl)amino] 2-methylidene4-oxobutanoic acid]

6. **Weak Interaction analysis by reduced Density Gradient (RDG) Method:** The interactions that exist between the methylene and carboxylic groups and the phenyl ring have been portrayed using the RDG approach. The nature of weak interactions within molecules is illustrated employing the RDG analysis. A variety of interactions may be extrapolated from the data with convenience. Low density and low gradient spikes were spotted in the scatter graph of the title compound's optimised configurations in Fig. 7, confirming an abundance of weak interactions. “The outcome of quantum chemical modelling were put through to weak interactions analysis making use of the reduced density gradient (RDG) algorithm of the Multiwfn software package. The RDG technique, which arises from the density and its first derivative (s = 1/2(32)1/3)/4/3), is a simple dimensionless variable in DFT used to outline departure away from a homogeneous electron distribution, where is the electron density, its reduced gradient,

and is the normalisation gradient. It is occasionally held to be that the diminished gradient employed in the above approach could end up in incredibly positive values in the density tails. (That is, an area far away from the molecule in which the density moves to zero exponentially)". Considering RDG in conjunction with the second the administrator local curvature of the electron density (r), one has the capacity to recognise between interactions deemed repulsive as well as those that tend to be enticing and to rank the relative potency of these interactions optically. Hydrogen bonds, Van der Waals contacts, and steric repulsion are only a few of the electronic phenomena that are represented by the non-covalent interactions description [28]. The benzene ring had a stronger steric influence than the carboxyl and methyl groups, as seen in Fig. 7. Strongly attractive interactions are implied by positive values of (2), whereas repulsive interactions are implied by negative values. A significant Van der Waals contact could be seen from the hue of the RDG isosurface between CH2 and COOH.

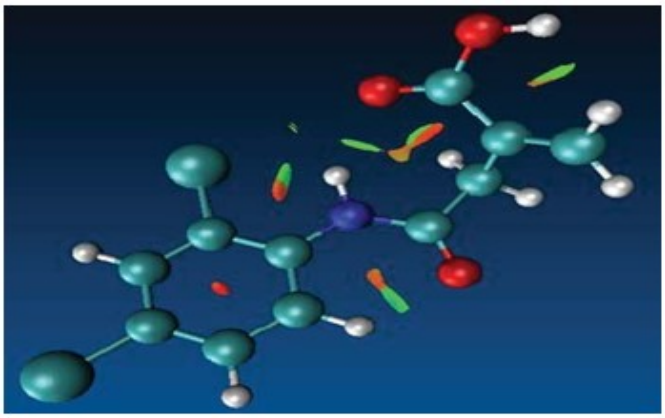

(a)

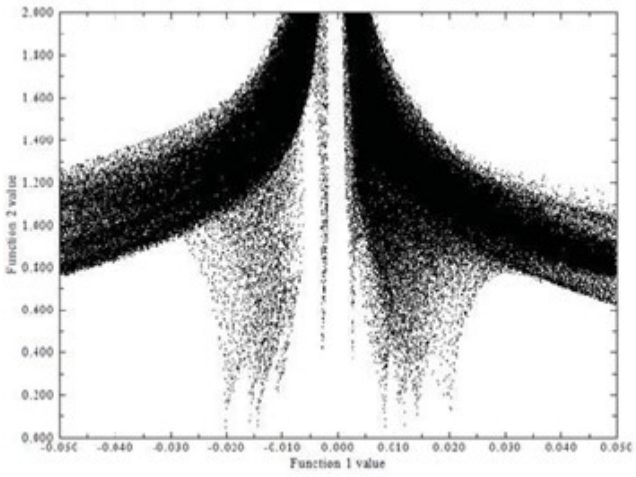

(b)

Figure7: (a) Plots of the RDG versus (2) pand (b) Colour scaling of interactions of[(2,4-dichlorophenyl)amino] 2-methylidene4-oxobutanoic acid

7. **Molecular Docking Study:** Automated docking was utilised for investigating the protein-drug interaction and figure out the path where the inhibitors link to the target protein's active site. A programme called Autodock 4.2 [8] was used for developing a genetic algorithm approach. The 2D (.mol) structures that comprise DPAB transform to 3D (.pdb) structures. From the protein data library, the protein structure file [37] was taken, and it modified through elimination of heteroatoms and adding C-terminal oxygen. The inhibitors were given Gasteinger partial charges, non-polar hydrogen atoms, and together non-polar hydrogen atoms for the docking calculations. All torsions were permitted to move around during docking. The protein residues resided at the exact middle of the grid map. “This included fifty docking runs, two hundred individuals that comprised the population of the evolutionary algorithm, and one thousand energy inspections. Protein inhibitor docking data confirmed the before talked about minimal docking energy, inhibition constant, and RMSD. The protein's molecular docking with DPAB supplied the best conformations plausible in terms of RMSD, inhibition constant, docking energy, binding energy, and intermolecular energy (Table 8). The Auto dock tool programme was applied to carry out molecular docking investigations. The active site was selected after the Rhinovirus target protein 1cqq [38] was obtained from Protein Data Bank (PDB ID 1CQQ). A molecular docking the test was conducted on the chemical subject of the title. The three-dimensional structure of a target receptor molecule is shown in Figure 8.8. The target protein is optimised on the basis of geometry”. In Discovery Studio, the title chemical is docked to an active site protein, delivering detail on the binding techniques. Of all active sites, the pocket with the most activity was found to include 58 amino acids. The root mean square deviation (RMSD) for the lowest docking energy determined to be 112.36 and the anticipated inhibition constant to be 797.29 M.

IV. CONCLUSION

By utilising FT-IR and FT-Raman, the current work has shed light on the spectroscopic characteristics of the compound in question, including optimised geometrical parameters, vibrational assignments, and electrical properties. The title molecule also revealed the necessary methods and theoretical research done by density functional theory. According to the combination of theoretical and practical knowledge, we were capable of entirely describe the vibrational assignments of the title molecule. The frontier energy gap in the molecule is established by charge transfer among the HOMO and LUMO energies. The homo-lumo band gap energy is 2.41 eV. The negative and positive parts of the molecule in the title were determined using a molecular electrostatic potential diagram. The lowest binding energy for the title chemicals to the protein, given by the molecular docking investigate is 5.17 kcal/mol.

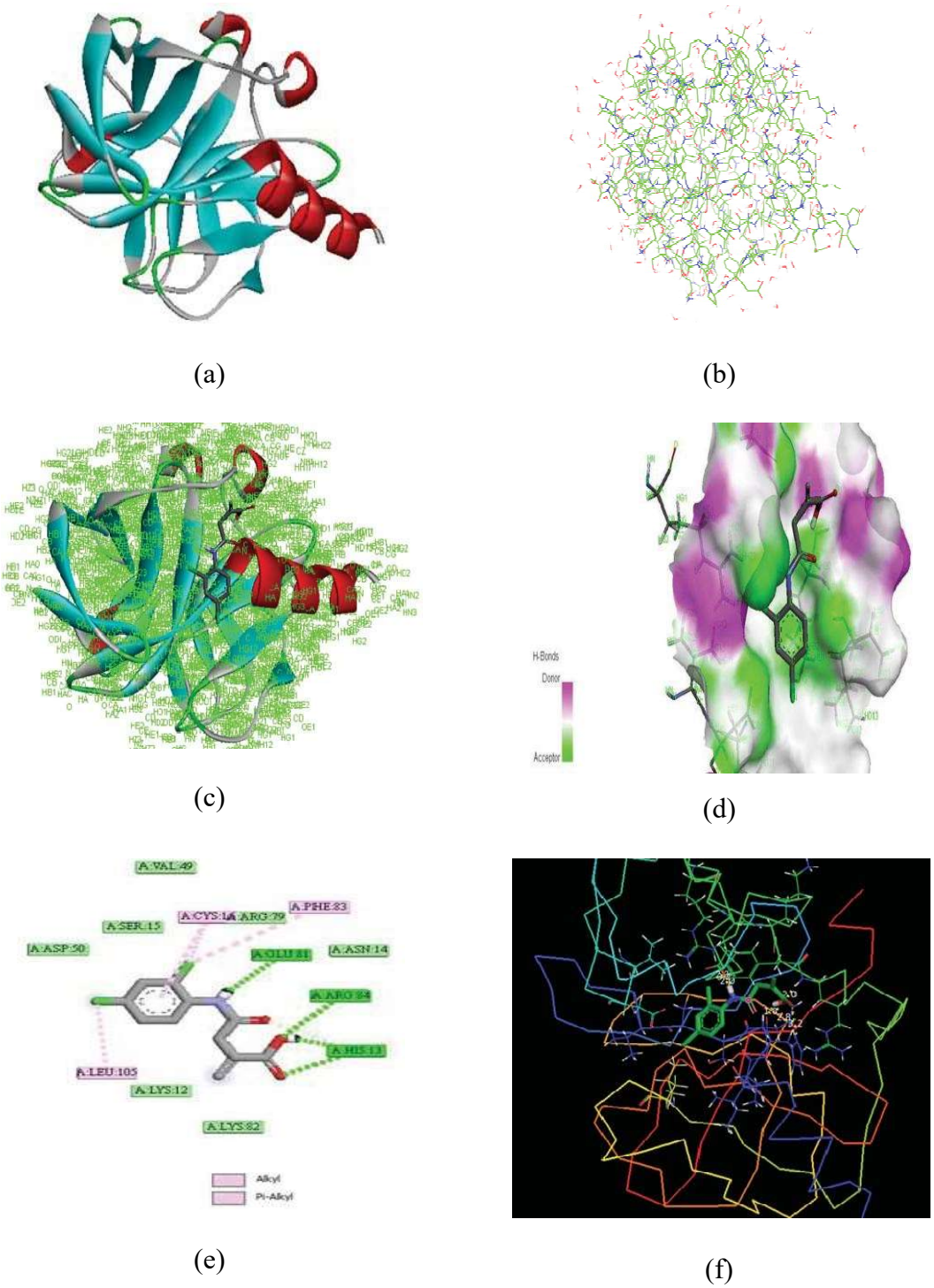

Figure 8: (a)Xray structure of protein (b)Adopted molecular system consists of drug molecule and amino acid residues (c)Protein-ligand docked pose (d)Surface view of protein-ligand (e) Different types of interactions formed between ligand-protein (f)Docked ligand embedded into the active site of protein

Table1: Optimized geometrical parameters of 4–[(2,4–dichlorophenyl)amino] 2–methylidene4–oxo but anoicacid, atom labeling according to Figure 8.1 Bond length(Å)

Parameters	6-311G++(d,p)	6-311G+(d,p)
C_1-C_2	1.41	1.41
C_1-C_6	1.41	1.41
C_1-N_{12}	1.41	1.41
C_2-C_3	1.39	1.40
C_2-Cl_{11}	1.76	1.76
C_3-C_4	1.39	1.40
C_3-H_{10}	1.08	1.08
C_4-C_5	1.39	1.40
C_4-Cl_9	1.76	1.76
C_5-C_6	1.40	1.40
C_5-H_8	1.09	1.08
C_6-H_7	1.08	1.08
Cl_{11}-O_{15}	5.29	5.28
Cl_{11}-O_{24}	3.58	3.52
N12-H13	1.02	1.02
N12-C14	1.37	1.37
C14-O15	1.23	1.23
C14-C16	1.54	1.54
O15-O24	4.59	4.60
C16-H17	1.09	1.09
C16-H18	1.09	1.09
C16-C19	1.52	1.52
C19-C20	1.34	1.34
C19-C23	1.50	1.50
C20-H21	1.09	1.09
C20-H22	1.09	1.09
C23-O24	1.22	1.22
C23-O25	1.36	1.36
O25-H26	0.97	0.97

Parameter	Bondangle (°)	
C_2-C_1-C_6	117.46	117.47
C_2-C_1-N_{12}	119.23	119.24
C_6-C_1-N_{12}	123.31	123.29
C_1-C_2-C_3	121.84	121.97
C_1-C_2-Cl_{11}	120.31	120.17
C_3-C_2-Cl_{11}	117.85	117.87
C_2-C_3-C_4	119.16	118.93
C_2-C_3-H_{10}	119.96	120.09
C_4-C_3-H_{10}	120.88	120.97

C_3-C_4-C_5	120.49	120.66
C_3-C_4-Cl_9	119.35	119.26
C_5-C_4-Cl_9	120.16	120.08
C_4-C_5-C_6	119.92	119.78
C_4-C_5-H_8	120.25	120.28
C_6-C_5-H_8	119.82	119.94
C_1-C_6-C_5	121.13	121.19
C_1-C_6-H_7	118.79	118.53
C_5-C_6-H_7	120.08	120.28
C_2-Cl_{11}-O_{25}	49.18	49.14
C_2-Cl_{11}-O_{24}	104.73	105.92
C1-N12-H13	116.44	116.50
C1-N12-C14	127.91	127.66
H13-N12-C14	115.54	115.75
N_{12}-$C1_4$-O_{15}	125.22	125.17
N12-C14-C16	114.45	114.54
O15-C14-C16	120.33	120.29
Cl11-O15-C14	35.60	35.72
C14-O15-O24	13.45	11.80
C14-C16-H17	105.39	105.48
C14-C16-H18	110.27	110.01
C14-C16-C19	112.70	112.99
H17-C16-H18	108.74	109.01
H17-C16-C19	109.60	109.50
H18-C16-C19	109.98	109.72
C16-C19-C20	122.41	122.58
C16-C19-C23	115.31	115.28
C20-C19-C23	122.09	122.01
C19-C20-H21	123.03	122.71
C19-C20-H22	120.90	120.83
H21-C20-H22	115.99	116.38
C19-C23-O24	121.99	122.06
C19-C23-O25	118.25	118.13
O24-C23-O25	119.76	119.81
Cl11-O24-C23	149.43	147.74
O15-C23-C24	76.07	76.48
C23-O25-H26	110.11	109.82

Table 2: Observed and calculated wave number and vibration assignments of 4–[(2,4–dichlorophenyl)amino] 2–methylidene4–oxobutanoicacid

Mode no	Calculated wavenumber (cm-1)		Observed wavenumber (cm–1)				Vibrational Assignments (PED %)
	FT–IR	FT-RAMAN	B3LYP/6-311++G(d,p)		B3LYP/6-311+G(d,p)		
			Scaled	Unscaled	Scaled	Unscaled	
1	3282		3758	3288	3825	3280	νOH(100)
2		3513	3494	3185	3513	3181	νNH(100)
3	3188		3269	3098	3275	3095	νCH(84)
4			3250	3089	3257	3088	νasCH2(97)
5	3074	3072	3233	3085	3245	3071	νCH(74)
6	3014		3222	3021	3233	3015	νCH(23)+νCC(21)
7		2993	3165	2995	3173	2991	νasCH2(38)+νCC(19)
8		2941	3156	2948	3164	2940	νCH2(52)+νNC(11)
9	2924		3091	2931	3103	2925	νCH2(62)+νNC(22)
10			1802	1718	1798	2915	νC=O(82)
11		1682	753	1683	1747	1680	νCO(70)+γCN(20)+δNH(10)
12	1630		1690	1635	1687	1630	νCC(71)+δscissCH(11)
13		1603	1639	1604	1640	1600	νC=C(100)+νOH(20)
14	1579		1622	1583	1620	1580	νCC(100)
15	1519		1565	1522	1562	1521	νCC(67)+δNH(13)
16	1474		1499	1476	1501	1475	δscissCH2(82)
17	1454		1494	1455	1483	1452	δscissCH2(82)
18	1395	1399	1460	1394	1450	1398	γOH(76)+δCH(10)
19	1348		1419	1351	1419	1350	βCH(57)+Ringγ(18)
20	1317		1376	1320	1370	1318	βCH(98)
21		1293	1336	1296	1336	1295	νCC(80)
22	1286		1322	1287	1315	1284	γwagCH2(88)
23			1297	1258	1296	1253	νCC(74)+δCCl(12)+νCN(10)
24	1231		1283	1233	1279	1230	γwagCH2(94)
25			1265	1208	1262	1206	νNC(58)
26			1248	1187	1246	1184	νasOH(43)+νOC(19)
27	1183	1148	1178	1151	1178	1150	βCH(14)+βCCC(14)
28			1169	1122	1167	1119	νasCC(62)+γwagCH2(18))
29	1101		1130	1104	1131	1102	γCC(60)+γCH(16)
30	1056		1120	1055	1119	1056	ρCH2(18))
31			1065	989	1063	988	γCC(60)+γCH(16)+γCO(10)
32		962	977	964	979	960	γCH(89)
33			976	940	978	943	γOH(88)
34	918		965	923	964	921	δwagCH2(94)
35	866	866	960	867	961	865	ρCH2(42)
36			945	855	944	854	γCH(42)+γCC(35
37			874	843	875	840	γCH(89)

38	822	825	866	826	866	825	γCCl(52)+γCO(20)+γCC(12)
39			841	815	841	812	γCH(89)
40			826	799	824	798	γCCl(61)+γRing(21)
41	785		812	788	811	786	ρCH2(61)
42	726		793	727	792	725	γNH(77)
43			739	684	746	683	γOH(51)
44		669	718	673	724	670	νCCl(81)
45	656		711	658	721	655	νCCl(81)
46			672	639	673	635	γCCl(66)
47	626		661	628	659	626	Ringγ(70)+γCN(18)
48	592		601	597	599	594	γCN(66)+γCO(18)
49	564		578	565	576	564	γCN(65)+γCO(18)+γCC(10)
50	564		568	548	568	548	γCN(65)+CO(18)+δCC(10)
51	547		542	515	540	511	βCCl(52)
52			519	490	508	487	γOH(57)+γCC(18)+νCC(10)
53			465	425	463	422	βCCl(46)
54			453	410	453	409	βCCl(65)
55		397	449	398	450	397	ρCH2(52)
56			396	385	396	383	Ringγ(52)+γCN(21)
57		361	375	362	374	360	Ringγ(66)+γCN(21)
58			359	319	362	316	γCC(57)+γCH2(20)
59			347	301	345	292	γCN(55)+γCC(21)+γCH(10)
60			303	278	302	276	γCC(53)+γCH2(18)
61		241	268	244	268	240	γCN(53)+νCC(20)+νCH(10)
62		220	245	230	243	222	γCC(53)+γCH2(18)
63		191	193	192	193	190	βCCl(11)
64			174	164	175	161	γCC(60)+γCO(18)
65			170	141	171	138	βCCl(11)
66		120	122	121	122	120	Ringbreathing(51)
67			115	112	113	109	δwagCH2+γCN(19)+γCC(12)
68			73	71	74	71	δRing(52)
69			62	61	66	60	γCCl(55)+γNH(19)
70			54	52	54	51	γCO(49)+γCC(23)+wCH2(10)
71			32	32	33	30	γCCl(53)+γNH(19)
72			16	5	17	15	γCO(50)+γNH(21)

ν −symmetricstretching,νas−asymmetricstretching,β−in-planebending,γ−out-ofplanebending,ρ−rocking,δwag−wagging,δsciss−scisssoring

Table 3: Second order perturbation theory analysis of 4–[(2,4–dichlorophenyl)amino] 2–Methylidene 4–oxobutanoic acid

Bond(A-B)	ED/e (a.u)	EDA %	EDB %	NBO	S%	P%
σC_1-C_2	1.97-	50.30	49.70	$0.70(sp^{1.73})+0.70(sp^{1.66})$	36.62	63.30
	0.04				37.63	62.30
σC_1-N_{12}	1.97-	37.98	62.02	$0.61(sp2.79)+0.78(sp^{1.83})$	26.34	73.52
	0.03				35.28	64.68
σC_2-C_3	1.97-	50.22	49.78	$0.70(sp^{1.63})+0.70(sp^{1.76})$	37.98	61.97
	0.02				36.14	63.78
σC_2-Cl_{11}	1.96-	44.99	55.01	$0.67(sp^{3.11})+0.74(sp^{6.23})$	24.26	75.55
	0.07				13.77	85.73
σC_4-Cl_9	1.97-	42.21	57.79	$0.64(sp^{3.30})+0.76(sp^{4.38})$	23.20	76.56
	0.03				18.50	81.04
C14-O15	1.98-	31.79	68.21	$0.56(SP^{2.22})+0.82(SP^{1.85})$	30.98	68.73
	0.02				35.04	64.85
C14-C16	1.97-	47.75	52.25	$0.69(SP^{1.71})+0.72(SP^{2.94})$	36.84	63.07
	0.05				25.39	74.54
C23-O25	1.98-	31.26	68.74	$0.55(SP^{2.52})+0.82(SP^{2.74})$	28.32	71.41
	0.07				26.71	73.19
$LP\sigma^{(Cl9)}$	1.98			$SP^{0.23}$	81.51	18.47
$LP\sigma^{(Cl11)}$	1.97			$SP^{0.58}$	63.21	36.78
$LP\sigma^{(O15)}$	1.95			$SP^{0.87}$	53.49	46.46
$LP\sigma^{(O24)}$	1.94			$SP^{0.76}$	56.69	43.28
$LP\sigma^{(O25)}$	1.97			$SP^{1.00}$	50.08	49.86

Table 4: Second order perturbation theory analysis of fock matrix in NBO analysis for4–[(2,4–dichlorophenyl) amino] 2–methylidene4–oxobutanoic acid

DonorNBO(i)	Acceptor NBO(j)	kcal/mol
σC_1-C_2	$\sigma^* C_3$-C_4	24.46
	$\sigma^* C_5$-C_6	18.79
σC_2-Cl_{11}	$\sigma^* C_1$-C_6	4.47
	$\sigma^* C_3$-C_4	4.39
σC_3-H_{10}	$\sigma^* C_1$-C_2	6.15
	$\sigma^* C_4$-C_5	5.67
σC_4-Cl_9	$\sigma^* C_2$-C_3	4.17
σC_5-H_8	$\sigma^* C_1$-C_6	5.45
	$\sigma^* C_3$-C_4	5.84
σC_{16}-H_{18}	$\sigma^* C_{14}$-O_{15}	6.19

	σ^*C_{19}-C_{20}	4.36
σC_{20}-H_{22}	σ^*C_{16}-C_{19}	7.06
	σ^*C_{19}-C_{23}	7.32
$LP\sigma Cl_{11}$	σ^*C_1-C_2	5.82
	σ^*C_{23}-O_{24}	6.37
$LP\pi Cl_{11}$	σ^*C_2-C_3	4.38
$LP\sigma N_{12}$	π^*C_1-C_2	28.38
	π^*C_{14}-O_{15}	28.44
$LP\sigma O_{15}$	π^*C_{14}-O_{15}	10.15
	π^*C_{23}-O_{24}	10.11
$LP\pi O_{15}$	σ^*N_{12}-C_{14}	18.82
	π^*C_{14}-O_{15}	7.65
	σ^*C_{14}-C_{16}	7.48
	π^*C_{23}-O_{24}	32.06
$LP\sigma O_{24}$	σ^*C_2-Cl_{11}	9.11
	σ^*C_{14}-O_{15}	5.30
	π^*C_{14}-O_{15}	9.13
	σ^*C_{19}-C_{23}	6.18
$LP\pi O_{24}$	σ^*C_2-Cl_{11}	6.35
	π^*C_{14}-O_{15}	28.71
	σ^*C_{19}-C_{23}	6.08
	π^*C_{23}-O_{24}	9.74
	σ^*C_{23}-O_{25}	19.57
$LP\sigma O_{25}$	σ^*C_{19}-C_{23}	6.21
$LP\pi O_{25}$	π^*C_{23}-O_{24}	28.45
	π^*C_{14}-O_{15}	8.17
	π^*C_{14}-O_{15}	132.45
	π^*C_{19}-C_{20}	26.09

Table 5: The charge distribution4–[(2,4–dichlorophenyl)amino]2–methylidene4–oxobutanoic acid of calculated by Mulliken charge method

Mulliken Charge(e)	
Atom	**(B3LP/6-311++G(d,p)**
C_1	0.51
C_2	-0.13
C_3	-0.23
C_4	-0.07
C_5	-0.21
C_6	-0.36
H_7	0.23
H_8	0.25
Cl_9	-0.09
H_{10}	0.28
Cl_{11}	0.05

N_{12}	-0.64
H_{13}	0.35
C_{14}	0.40
O_{15}	-0.30
C_{16}	-0.51
H_{17}	0.24
H_{18}	0.26
C_{19}	0.12
C_{20}	-0.58
H_{21}	0.19
H_{22}	0.24
C_{23}	0.36
O_{24}	-0.25
O_{25}	-0.54
H_{26}	0.42

Table 6: Molecular propertis of 4–[(2,4–dichlorophenyl)amino] 2–methylidene4–oxobutanoic acid

Molecular Properties	Energy gap (eV)	Ionization potential (I)	Electron Affinity (A)	Glopal Hardness (η)	Electro Negativity (χ)	Chemical Softness (σ)	Chemical potential (μ)
		(eV)	(eV)	(eV)	(eV)	(eV)	(eV)
E_{HOMO}	2.41	0.17	0.08	0.04	0.12	22.49	-0.13
E_{HOMO-1}	4.62	0.21	0.04	0.12	0.13	15.23	-0.12
E_{HOMO-2}	5.85	0.24	0.01	0.13	0.14	9.08	-0.11

Table 7: Bond distance between ligand and residues

Ligand	Protein PDBID (IFZV)	
	Residues	Bond Distance
4–[(2,4–dichlorophenyl)amino]2–methylidene4–oxobutanoicacid	TYR35/O	2.1Å
	GLU39/HN	2.0Å
	LYS52/HZ2	1.9Å
	GLY/38CA	3.0Å
	GLY38/HN	1.9Å
	LYS/HD1	2.0Å
Estimated inhibition constant		797.29μM
Total internal energy		-0.42kcal/mol
Electrostatic energy		-1.30kcal/mol
Binding energy		-5.47kcal/mol
RMSD		112.36Å

REFERENCE

[1] M.L. Shaw, Rev. Med. Virol 21 (2011) 358.
[2] M.S. Diaramond, M. Farzan, Nat. Rev. Immunol. 13 (2013) 46.
[3] Y. Debing, D. Jochmans, J. Neyts, Curr. Opin. Virol 3 (2013) 217.
[4] Y. Zhou, G. Simmons, Expert, Rev. Anti. Infect. Ther. 10 (2012) 1129.
[5] M.J. Frisch, G.W. Trucks, H.B. Schlegel, G.E. Scuseria, M.A. Robb, J.R. Cheeseman, V.G. Zakrzewski, J.A. Montgomery, Jr., R.E. Stratmann, J.C. Burant, S. Dapprich, J.M. Millam, A.D. Daniels, K.N. Kudin, M.C. Strain, O. Farkas, J. Tomasi, V. Barone, M. Cossi, R. Cammi, B. Mennucci, C. Pomelli, C. Adamo, S. Clifford, J. Ochterski, G.A. Petersson, P.Y. Ayala, Q. Cui, K. Morokuma, D.K. Malick, A.D. Rabuck, K. Raghavachari, J.B. Foresman, J. Cioslowski, J.V. Ortiz, A.G. Baboul, B.B. Stefanov, G. Liu, A. Liashenko, P. Piskorz, I. Komaromi, R. Gomperts, R.L. Martin, D.J. Fox, T. Keith, M.A. Al-Laham, C.Y. Peng, A. Nanayakkara, M. Challacombe, P.M.W. Gill, B. Johnson, W. Chen, M.W. Wong, J.L. Andres, C. Gonzalez, M. Head-Gordon, E.S. Replogle, J.A. Pople, Gaussian 09, B.01 Revision, Gaussian Inc., Wallingford, CT, 2010.
[6] H.T. Varghese, C.Y. Panicker, D. Philip, J. Raman Spect. 38 (2007) 309.
[7] B.Smith, Infrared spectral interpretation, CRC Press,Boca Raton, 1999.
[8] O.Trott, A.J.Olson, J.Comput. Chem.31(2010)455.
[9] T.Rajamani, S.Muthu, SolidStateSci.13(2013)90.
[10] P.Skyes, A guide book to mechanis minorganicchemistry,6thEd.,Pearson Education, India, New Delhi, 2004.
[11] Sidir, Y.G.Sidir,E.Tasal,C.V.Ogretir,J.Mol.Struct.2013(2012)67.
[12] D.A. Matthews, P.S. Dragovich, S.E. Webber, S.A. Fuhrman, A.K. Patick, L.S. Zalman, T.F. Hendrickson, R.A. Love, T.J. Prins, J.T. Marakovits, R. Zhou, J. Tikhe, C.E. Ford, J.W. Meador, R.A. Ferre, E.L. Brown, S.L. Binford, M.A. Brothers, D.M. DeLisle, S.T. Worland, Proc. Natl. Acad. Sci. USA 96 (1999) 11000.
[13] R. Ditchfield, J. Chem. Phys. 56 (1972) 5688.
[14] O. Hernandez, K.S. Knight, W. Van Beek, A. Boucekkine, A. Boudjada, Paulus, J. Meinnel, J. Mol. Struct. 791 (2006) 41.
[15] J.R. Durig, T.S. Little, T.K. Gounev, J.K. Gardner, J.F. Sullivan, J. Mol.Struct. Theochem. 375(1996)83.
[16] S. Kundoo, A.N. Banarjee, P. Saha, K.K. Chattopadhyaya, Mater Lett. 57 (2003) 2193.
[17] W. Wattanathana, N. Nootsuwan, C. Veranitisagul, N. Koonsaeng, S. Suramitr, A. Laobuthee, S. Murugavel S. Sundaramoorthy, D. Lakshmanan, R. Subahashini, P. Pavan Kumar, J. Mol. Struct. 1131 (2017) 51.
[18] M.Silverstein, G.C.Basseler, C.Morill, Spectrometric identification of organic compounds, Wiley, NewYork, 1981.
[19] N.Subramani,N. Sundaraganesan, S.Sudha, V.Arulmozhi, G.D.Sockalingam, M.Bergamin, Spectrochim. ActaA78(2011)1058.
[20] F.Jian ,P.Zhou, H.Guo, Y.Li,Spctrochim. ActaA69(2008)647.
[21] L.J.Bellamy, ThirdEd. ,Chapmanand Halls, London,1975.
[22] C.S.Hiremath, T.Sundius, Spectrochim. ActaA74(2009)1260.
[23] E.D. Glendening, A.E.Reed, J.E.Carpenter, F.Weinhold, NBO Version3.1, Theoretical chemistry institute and department of chemistry, University of Wisconsin, Madison, 1988.
[24] M.Mushtaque, M.Jahan, M.Ali, M.ShahzadKhan, M.ShahidKhan,P. Sahay, A.Kesarwani,J. Mol.Strct.1122(2016)164.
[25] S.Fliszar,ChargedistributionsandchemicalEffects,Springer,NewYork,1983
[26] Sponer, P.Hobza,Int.J.Quantum.Chem.57(1996)959..
[27] Fleming, Frontier orbitals and organic chemical reactions,Wiley, London, 1976.
[28] D.Li,Y.Yang, C.Li,Y.Liu, J.Lumins.182(2017)15.
[29] D.A.Kleinmann,Phys. Rev.126(1962)1977.
[30] R.K.Roy, H.Hirao, S.Krishnamoorthy, S.Pal, J.Chem. Phys.115(2001)2901.
[31] M.Adant, L.Dupuis, L.Bredas, Int.J.QuantumChem.56(2004)497.
[32] P.Bultnick, R.Carbo-Dorca, W.Langenaekar,J.Chem.Phys.118(2003)4349.
[33] R.G.Parr ,W.J.Yang, J.Am.Chem.Soc.106(1984)4049.
[34] R.G.Parr, W.Yang, Density functional theory of atomsand molecules, Oxford University Press, New York,1989.

[35] P.W.Ayers, R.G.Parr, J.Am.Chem. Soc.122(2000)2010.
[36] P.Kolandaivel, G.Parveen, P.Selvarengan, J.Chem.Sci.117(2005)591.
[37] http://www.rcsb.org/pdb/home/home.do.
[38] D.A.Matthews,P.S.Dragovich,S.E.Webber,S.A.Fuhrman,A.K.Patick, L.S.Zalman, T.F. Hendrickson, R.A.Love, T.J.Prins ,J.T.Marakovits, R.Zhou, J.Tikhe, C.E.Ford, J.W.Meador, R.A.Ferre, E.L.Brown, S.L.Binford,M.A.Brothers,D.M.DeLisle,S.T.Worland,Proc.Natl.Acad. Sci.USA 96(1999) 11000.

